PHYSICAL REVIEW B **87**, 115209 (2013)

Comprehensive picture of *p*-type doping of P3HT with the molecular acceptor F_4TCNQ

P. Pingel and D. Neher*

Soft Matter Physics, Institute of Physics and Astronomy, University of Potsdam, Karl-Liebknecht-Str. 24-25, D-14476 Potsdam, Germany

(Received 1 February 2013; published 28 March 2013)

By means of optical spectroscopy, Kelvin probe, and conductivity measurements, we study the *p*-type doping of the donor polymer poly(3-hexylthiophene), P3HT, with the molecular acceptor tetrafluorotetracyanoquinodimethane, F_4TCNQ, covering a broad range of molar doping ratios from the ppm to the percent regime. Thorough quantitative analysis of the specific near-infrared absorption bands of ionized F_4TCNQ reveals that almost every F_4TCNQ dopant undergoes integer charge transfer with a P3HT site. However, only about 5% of these charge carrier pairs are found to dissociate and contribute a free hole for electrical conduction. The nonlinear behavior of the conductivity on doping ratio is rationalized by a numerical mobility model that accounts for the broadening of the energetic distribution of transport sites by the Coulomb potentials of ionized F_4TCNQ dopants.

DOI: 10.1103/PhysRevB.87.115209 PACS number(s): 81.05.Fb, 68.55.Ln, 72.80.Le, 73.61.Ph

I. INTRODUCTION

Intentionally doped organic semiconductors are nowadays commonly used as transport and injection layers in state-of-the-art organic electronic devices.[1] Being the key concept for the versatility of inorganic semiconductors, controlled doping suggests tremendous benefit by enabling the tuning of the organic semiconductor's electrical, optical, and morphological properties.

Stable doping of organic semiconductors has been realized by adding strong molecular donors or acceptors to conjugated small molecules or polymers. In particular, 2,3,5,6-tetrafluoro-7,7,8,8-tetracyanoquinodimethane (F_4TCNQ) has been used as electron acceptor to *p* dope evaporated[2–6] and solution-processed[7–16] organic semiconductors due to its high electron affinity of 5.24 eV.[2] Upon doping the prototypical polymeric semiconductor poly(3-hexylthiophene) (P3HT) with F_4TCNQ, electrical conductivities up to 100 S/m have been reported.[7]

It is well established that the doping effect, i.e., the increase of the majority charge carrier density, is based on a charge transfer reaction involving an appropriate donor and acceptor. Two contradictory models that are commonly used to explain the donor-acceptor ground-state interaction are sketched in Fig. 1 using the example of P3HT being doped with F_4TCNQ. In the integer charge transfer model [see Fig. 1(a)], an electron is completely transferred from P3HT to the F_4TCNQ acceptor. Since the concentration of F_4TCNQ in the P3HT matrix is typically low (usually a few mol % or below), it is expected that the transferred electron remains fixed at the F_4TCNQ molecule. The associated hole on P3HT can be either Coulombically bound by the F_4TCNQ anion or may move freely within the matrix of P3HT. The notion of a strong Coulomb binding is in line with the peculiar observation that the free-charge carrier density is often far lower than the dopant concentration.[13,17–20] The strong Coulomb binding is mediated by the low permittivity in organic semiconductor solids. In contrast, it has been reported that the free-charge carrier density does not depend on temperature in some F_4TCNQ-doped small-molecule organic semiconductors.[3,5,6] This has been explained in terms of the entire ionization of all applied acceptors and, if at all, the only shallow trapping of the doping-induced majority charge carriers.

Figure 1(b) illustrates an alternative model of molecular doping that relies on the formation of hybrid charge transfer complexes upon the interaction of the donor and acceptor. Based on density functional theory, studies using a quaterthiophene model for P3HT and F_4TCNQ as dopant, Aziz *et al.*[7] suggested partial charge transfer between these donor and acceptor species and that a supramolecular charge transfer complex (CTC) is formed whose highest occupied and lowest unoccupied molecular orbitals, HOMO and LUMO, respectively, are derived from both the neutral P3HT HOMO and F_4TCNQ LUMO. Similar results have been obtained for a number of F_4TCNQ-*p*-doped oligothiophenes and pentacene and for naphthalene-tetracaboxylic-dianhydride (NTCDA) *n*-doped with a tetrathiafulvalene (TTF) derivative.[21,22] In this model, holes are created due to the electron deoccupation of P3HT HOMOs (and electron occupation of CTC LUMOs) as a consequence of Fermi-Dirac statistics. Whether these holes are free or Coulombically bound to charged CTCs is open to question.

In a previous report, we characterized the free-hole density and conductivity of P3HT layers that have been doped by F_4TCNQ at low to moderate dopant concentrations, i.e., in the ppm to per mill regime. We found that only 5% of the F_4TCNQ dopants took effect in creating free holes that contribute to electrical conduction. Moreover, we found that the conductivity increases sublinearly (with an exponent of approximately 0.6) with doping ratio. The latter is in conflict with the frequent observation of a superlinear increase of the conductivity, which has been related to trap filling by the doping-induced charge carriers[1] or an increase of permittivity in highly doped layers.[20]

Here, we aim at understanding the process of doping P3HT with F_4TCNQ and the electrical characteristics of such doped layers by means of optical absorption spectroscopy, surface potential measurements, and conductivity measurements of hole-only devices. We can now confirm that the concentration of ionized F_4TCNQ molecules is (within an error of 50%) given by the molecular ratio of the donor and acceptor in solution, meaning that most acceptor molecules are incorporated into the layer and that almost every F_4TCNQ dopant undergoes integer charge transfer with a P3HT donor site. Therefore the low concentration of mobile holes implies that

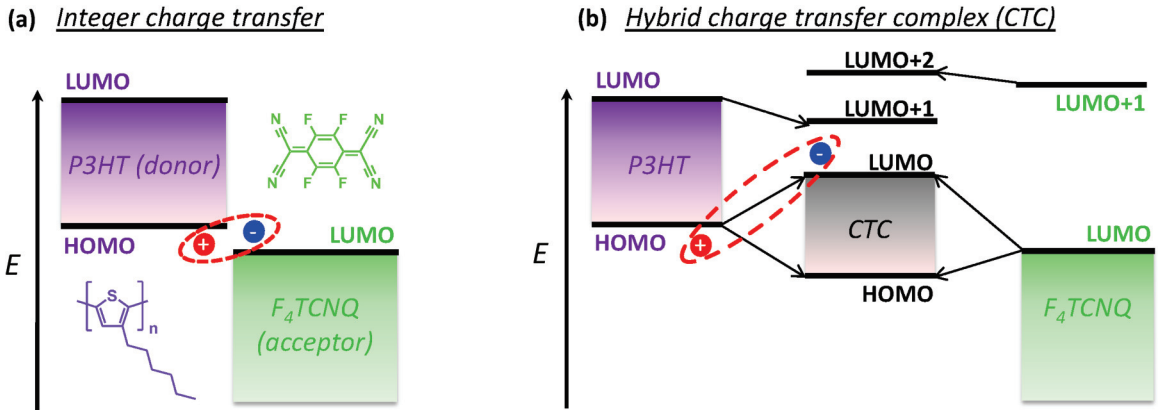

FIG. 1. (Color online) Contradictory models of the charge transfer between P3HT and F_4TCNQ. (a) Integer charge transfer model that presumes full ionization of donor and acceptor, resulting in a hole-F_4TCNQ anion pair that is bound or can split up. (b) Hybrid charge transfer model according to Ref. 7, which presumes the formation of hybrid supramolecular orbitals upon electronic interaction of P3HT and F_4TCNQ. Free-charge generation might occur by intermolecular excitation involving the HOMO of unreacted P3HT and the LUMO of a nearby CTC.

most of the created P3HT polarons remain strongly bound to a F_4TCNQ anion. The electrical conductivity turns from a sublinear increase at low to moderate doping ratios towards a superlinear increase at high doping ratios in the mol% regime. This dependency is quantitatively reproduced by a numerical mobility model of Arkhipov *et al.*,[23,24] which considers the broadening of the energetic landscape for charge transport upon doping by the Coulomb potential of the left-behind F_4TCNQ anions.

II. EXPERIMENT

F_4TCNQ has been obtained and used as received from Sigma-Aldrich. Our P3HT sample is a molecular weight fraction ($M_w = 35.8$ kg/mol, $M_n = 27.0$ kg/mol) with deuterated hexyl side chains for prospective neutron scattering experiments. Our extensive previous investigations show that the structural and electronic properties are not altered by the deuteration and that the performance of this P3HT fraction is outstanding in field-effect devices.[25–27] Doped samples have been prepared by mixing separate chloroform solutions of P3HT and F_4TCNQ according to the desired doping ratio χ. A doping ratio of, for instance, 1:1000 means that one F_4TCNQ molecule is added per 1000 thiophene repeat units of P3HT and is equivalent to $\chi = 10^{-3}$.

UV-Vis-NIR absorption spectra have been recorded with a Cary 5000 photospectrometer. Solution samples were prepared from 2 and 0.5 g/l solutions of P3HT and F_4TCNQ, respectively. The optical path length of the quartz cuvette was 1 mm and 10 mm, respectively. The presented solution spectra are the averages of five consecutive scans in order to reduce the noise in the NIR. Solid samples have been prepared on glass substrates after cleaning with common organic solvents in an ultrasonic bath. Sample solutions, based on 10-g/l P3HT and 0.5-g/l F_4TCNQ in chloroform, were spin coated on the glass substrates at 1000 rpm for 30 sec in inert N_2 atmosphere, yielding layers with a thickness of typically ~100 nm. Film spectra have been recorded using an integrating sphere in order to account for light scattering and reflection. The presented spectra are based on the averages of ten consecutive transmission/reflection scans.

Surface (Kelvin) potential measurements of undoped and doped layers on metal substrates have been repeatedly performed in the dark using a SKM KP 4.5 (KP Technology Ltd.) with 2-mm probe diameter in a N_2-filled glovebox with <1 ppm O_2 and H_2O contamination. Typically, fresh samples were stored in the glovebox for 30 min prior to the measurement in order to allow for degassing of residual solvent traces. Calibration of the tip work function was done against highly ordered pyrolytic graphite (HOPG), for which we assumed a work function of 4.6 eV.[28] Metal electrodes have been prepared on cleaned glass substrates. The glass surface was precovered with a smoothing layer of the PEDOT:PSS formulation Clevios™ P VP AI 4083 by spin-coating at 5000 rpm for 30 sec and subsequent annealing at 180 °C for 10 min. Then, 50 nm of aluminum or copper was evaporated under high-vacuum conditions. Sample preparation and handling continued in N_2 atmosphere. Undoped and doped P3HT layers were deposited by spin-coating at 1500 rpm for 30 sec. Solutions were based on 0.5–25-g/l P3HT and 0.02–0.5-g/l F_4TCNQ in chloroform, depending on the desired layer thickness. Note that the present preparation conditions typically result in layer structures with a considerable amount of disordered material and, therefore, random molecular orientations.[16,25,27] Due to the large probe diameter, the surface potential data represent macrocopic means across these portions of the layer surfaces.

Current-voltage characteristics have been recorded with a Keithley 2400 source-measure unit. Hole-only devices were prepared on glass substrates with patterned indium-tin-oxide electrodes. After oxygen plasma treatment at 200 W for 3 min, Clevios™ P VP AI 4083 PEDOT:PSS has been spin-coated at 1500 rpm for 30 sec, followed by annealing at 180 °C for 10 min. Sample preparation continued under inert conditions. Undoped and doped P3HT layers were spin-coated at 500 rpm for 30 sec from solutions based on 30-g/l P3HT and 0.5-g/l F_4TCNQ, yielding thick layers in the range of 250–900 nm similar to our previous metal-insulator-semiconductor devices.[15] The samples were completed by evaporation of 5-nm MoO_3 and 100-nm Al as top electrodes. The devices have been encapsulated using Araldite 2011 two-component epoxy resin and measured outside the glovebox.

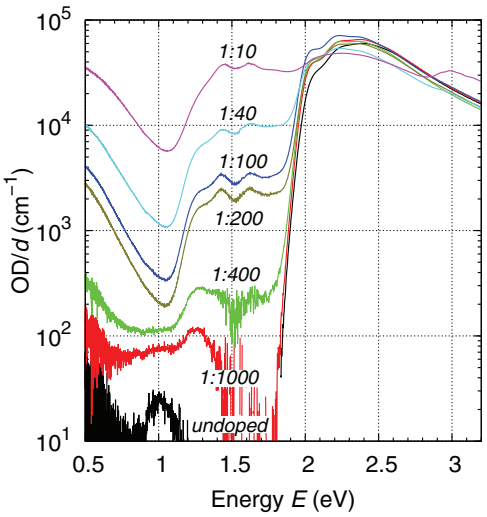

FIG. 2. (Color online) Thickness-normalized absorbance of undoped and F_4TCNQ-doped P3HT layers.

III. RESULTS & DISCUSSION

A. Optical spectroscopy

In order to gather information on the nature of the F_4TCNQ-P3HT charge transfer, we performed UV-Vis-NIR absorption spectroscopy on thin films and in solution. Figure 2 shows the optical absorbance normalized by layer thickness of undoped and F_4TCNQ-doped P3HT layers. The thickness of these layers was typically around 100 nm. Upon doping, a pronounced subband gap absorption occurs in addition to the absorption of undoped P3HT. A qualitative comparison of the NIR region to published spectra of P3HT polarons[29,30] and fully ionized F_4TCNQ anions[31,32] allows a clear assignment of the prominent 1.43 and 1.62 eV peaks to the absorption of singly negatively charged F_4TCNQ. The rectangular-shaped broad band between 1.2 and 1.8 eV and the increasing absorption below 1 eV are typical features of polarons in P3HT. Note that if the F_4TCNQ-P3HT charge transfer resulted in hybrid supramolecular species with partial electron transfer, their spectra should be severely different from the observed case. In particular, these species would introduce new absorption transitions between their hybrid supramolecular orbitals.

In order to quantify the absolute concentration of ionized acceptors formed in blends of F_4TCNQ and P3HT, we decompose the NIR absorption into the P3HT polaron and F_4TCNQ anion parts. For this analysis, suitable reference spectra of the charged compounds are essentially needed. Unfortunately, spectra and absolute values of the extinction coefficients (or absorption cross-sections) of P3HT[29,30,33–36] and F_4TCNQ polarons in solid thin films are not consistent or not available. Moreover, the P3HT polaron absorption is very sensitive to the layer's preparation conditions and the properties of the specific P3HT sample, rendering a meaningful algebraic decomposition difficult. We, therefore, start by analyzing the absorption spectra of F_4TCNQ-P3HT blends in chloroform solution.

The spectra of F_4TCNQ-P3HT chloroform solutions with varied doping ratios are displayed in Fig. 3(a). Qualitatively, the solution spectra coincide with the spectra of the doped layers, meaning that charge transfer takes place already in solution upon the admixture of F_4TCNQ and P3HT. In more detail, the solution spectra reveal a further distinct absorption feature at 2.0 eV which is only present if F_4TCNQ was added. This transition is hidden in the thin-film spectra by the strongly red-shifted absorption of neutral planarized P3HT.

Next, we reconstruct the NIR absorption of the doped solution spectra by weighted sums of a F_4TCNQ anion and a P3HT polaron reference spectrum. An example of the reconstruction of the 1:100-doped sample is plotted in Fig. 3(b). As a reference for the extinction of F_4TCNQ anions we use the molar extinction coefficient spectrum published in Ref. 32. There, the extinction coefficients of neutral, singly, and doubly ionized F_4TCNQ bound in charge-transfer salt crystals are reported. The advantage of using these spectra is that the amount of ionized F_4TCNQ is exactly known from

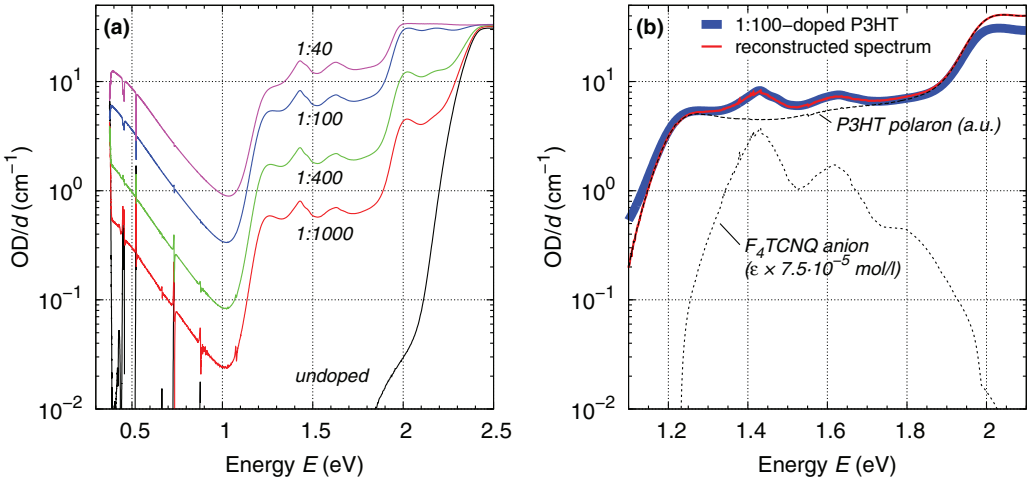

FIG. 3. (Color online) (a) Absorbance per length of pure (undoped) P3HT and mixtures with F_4TCNQ (molar mixing ratios given in the figure) in chloroform solution. The undoped sample had a concentration of 2-g/l P3HT in chloroform. Absorbance is cut off beyond 2 eV for the 1:40-doped sample due to instrumental limitations. (b) Reconstruction of the P3HT polaron/F_4TCNQ anion absorption of the 1:100-doped P3HT sample from reference spectra. The F_4TCNQ anion spectrum is reprinted with permission from Ref. 32. Copyright 1989 American Chemical Society.

TABLE I. Concentrations of ionized F_4TCNQ found in a mixture of F_4TCNQ and P3HT in chloroform at various doping ratios.

Doping ratio	P3HT[a] repeat units (10^{-2} mol/l)	F_4TCNQ[a] (10^{-5} mol/l)	F_4TCNQ^-[b] (10^{-5} mol/l)	Ionized fraction
1:1000	1.19	1.19	0.6	0.50
1:400	1.18	2.96	2.0	0.68
1:100	1.13	11.3	7.5	0.66
1:40	1.03	25.8	18	0.70

[a]Intentionally applied amount in solution.
[b]Measured by decomposition of the optical spectra.

stoichiometry. A comparison between the reported spectra and our own absorption measurements of neutral F_4TCNQ in chloroform solution gives a close absolute agreement of the spectral shape and extinction coefficients. Another solution sample with a high but unknown amount of ionized F_4TCNQ matches the spectral shape of the crystal reference spectrum with respect to the anion absorption bands in the NIR (see Supplemental Material[37] and Ref. 32 therein). A P3HT polaron reference spectrum was realized by doping the neutral P3HT powder in saturated iodine vapor. The exposed powder was then dissolved into chloroform at a concentration of 0.025 g/l (higher concentrations were not possible due to the limited solubility of the doped compound).

The algebraic reconstruction of the F_4TCNQ-P3HT blend spectra in solution allows for an estimate of the F_4TCNQ anion concentration. Table I compares these values with the concentrations of actually applied F_4TCNQ upon blending with P3HT. Approximately 50–70% of the initial quantity of F_4TCNQ is retrieved as anions. As expected, this ionization efficiency is lower in very dilute solutions (see Supplemental Material[37] and Ref. 38 therein). Assuming that the F_4TCNQ anion and donor-acceptor charge transfer pair concentrations are equal, we can now calculate the molar extinction coefficient of the charge transfer pairs. At 1.52 eV, the notable minimum in between the two major F_4TCNQ anion peaks, the molar extinction coefficient amounts to $(8.3 \pm 1.8) \times 10^4$ l/mol/cm. We use this value for a rough estimate of the concentration of donor-acceptor pairs that have undergone charge transfer in the F_4TCNQ-doped P3HT layers, the results of which are summarized in Table II.

It turns out that the concentration of ionized F_4TCNQ is only little lower than the molecular concentration calculated from the molar mixing ratio in solution (assuming a mass density of 1.1 g/cm^3 of the solid film[39]). This means that the majority of the applied F_4TCNQ acceptor molecules undergoes integer charge transfer with P3HT. This is a vitally important finding, because it is usually found from electrical and electrostatic measurements that the density of doping-induced free holes is drastically lower than the dopant density,[13,17–20] as we will also show in the following. By the same token, the significant formation of isolated clusters of F_4TCNQ, which has been suggested to explain the reduced free-charge carrier density by some authors[14,40] and has been excluded by others,[1,8,16] can be ruled out here as well.

TABLE II. Concentrations of ionized F_4TCNQ found in F_4TCNQ-doped P3HT layers at various doping ratios.

Doping ratio	F_4TCNQ^-[a] (m^{-3})	F_4TCNQ[b] (m^{-3})	Ionized fraction
1:200	$(1.5 \pm 0.3) \times 10^{25}$	2×10^{25}	0.77 ± 0.17
1:100	$(2.0 \pm 0.5) \times 10^{25}$	4×10^{25}	0.51 ± 0.11
1:40	$(6.3 \pm 1.3) \times 10^{25}$	1×10^{26}	0.64 ± 0.14
1:10	$(2.7 \pm 0.6) \times 10^{26}$	4×10^{26}	0.67 ± 0.15

[a]Measured by analysis of the optical spectra in Fig. 2.
[b]Intentional amount according to the doping ratio, assuming a mass density of P3HT[39] of $\rho = 1.1$ g/cm^3.

B. Surface (Kelvin) potential measurements

Generally, a comparison of the surface potentials of an uncovered conductive substrate and the same substrate coated with a polymer yields combined information on the interface energetics and on the electronic structure of the polymer bulk.[41,42] As we have shown recently, deposition of an undoped conjugated polymer on an electrode with sufficiently small work function leads to electron transfer from the electrode into tail states of the polymer's lowest unoccupied molecular orbital (LUMO) manifold (see Fig. 4, left panels). This process is accompanied by a continuous increase of the work function of the sample (band bending) with increasing polymer layer thickness.[43] From a numerical analysis of the band bending, quantitative information on the density of tail states (DOTS) can be obtained. Similar to this, deposition of the same polymer on an electrode with sufficiently high work function induces holes into the polymer and allows for measuring the DOTS derived from the HOMO manifold.

Experimental work functions at the surface of undoped P3HT layers with varied thicknesses are plotted as solid black symbols in Fig. 5(a). These measurements have been performed with layers on aluminum ($\Phi_{Sub} \approx 3.15$–3.3 eV, upper circles) and on copper ($\Phi_{Sub} \approx 4.5$–4.6 eV, lower triangles). Note that the work functions of the covered metal electrodes can be offset from that of the bare metals due to the formation of interface dipoles.[44] As for other conjugated polymers, we find that the sample work function increases with P3HT thickness on aluminum, while it decreases on copper. The observation that both work function curves tend to saturate at well-separated values is consistent with the injection of electrons into LUMO-derived states on aluminum and the injection of holes into HOMO-derived states on copper, as explained above.

As seen in Fig. 5(a), the course of the work function of F_4TCNQ-doped P3HT on aluminum as a function of film thickness is qualitatively different from the undoped samples. When a *p*-doped layer is deposited onto a low work function metal such as aluminum, a classical Schottky contact is formed. Thereby, mobile doping-induced holes in the HOMO distribution of P3HT drift towards the aluminum contact and get neutralized at the metal interface. The immobile F_4TCNQ anions are left behind and form a negatively charged depletion zone (see Fig. 4, right panels). If all holes created by doping were extracted, the charge density in the depletion zone would be determined by the total density of ionized F_4TCNQ. We will show later that this is not the case in F_4TCNQ-doped P3HT

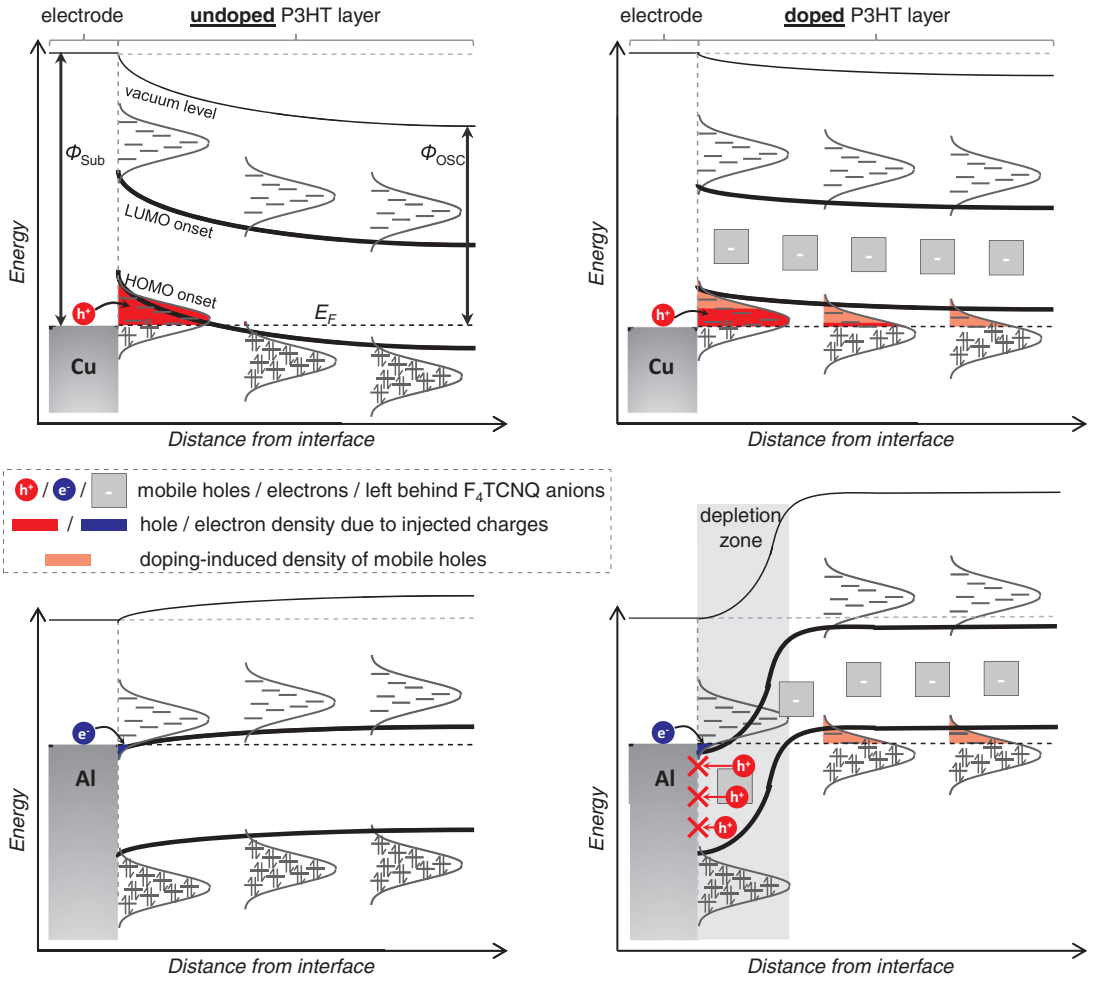

FIG. 4. (Color online) Scheme of the electron and hole transfer of undoped (left) and doped (right) P3HT layers on high (Cu, top) and low work function (Al, bottom) metal substrates.

layers. For layer thicknesses that are thinner than the depletion zone width, the work function curve has a parabolic shape [see Fig. 5(a)], which implies a homogeneous distribution of F_4TCNQ in the sample. From the width of the depletion layer, the anion density—and, therefore, the mobile-hole density—can be calculated. For larger layer thicknesses, the work function of doped P3HT layers on both aluminum and copper will merge to a common value, which is the bulk Fermi level of the doped semiconductor. Note that this value is about 4.45 eV, which is well within the tail of the typical distribution of HOMO levels in P3HT. However, the change of the surface potential of P3HT on aluminum is rather gradual. In order to gather information on the density-of-states (DOS) distributions and the hole densities in the polymer layers, we have numerically analyzed the work function versus layer thickness curves following the general procedures by Lange *et al.*,[43] but now including doping.

The surface potential is measured using the capacitor-like configuration of a Kelvin probe setup. The potential difference between the sample and a reference tip is adjusted such that the gap in between those is field free. The electrical potential $\phi(x)$ in the polymer layer hence follows the Poisson equation

$$\frac{d^2\phi}{dx^2} = \frac{e}{\epsilon_r \epsilon_0}[n(x) - p(x) + N_a] \tag{1}$$

with the boundary condition $\frac{d\phi}{dx}(L) = 0$, where $n(x)$ and $p(x)$ are the electron and hole densities in the LUMO and HOMO, respectively, N_a is the density of ionized F_4TCNQ acceptor molecules, x is the distance from the electrode, L is the total layer thickness, and $\epsilon_r = 3.5$ is the relative permittivity. The equilibrium local charge densities are related to the HOMO- and LUMO-derived density-of-states (DOS) distributions g_{HOMO} and g_{LUMO}, the Fermi level E_F, and the local potential according to

$$n(x) = \int_{-\infty}^{\infty} \frac{g_{\mathrm{LUMO}}[E + e\phi(x)]}{1 + \exp\left(\frac{E - E_F}{k_B T}\right)} dE \quad \text{and} \tag{2}$$

$$p(x) = \int_{-\infty}^{\infty} \frac{g_{\mathrm{HOMO}}[E + e\phi(x)]}{1 + \exp\left(\frac{E_F - E}{k_B T}\right)} dE. \tag{3}$$

Due to the large reservoir of electrons, the common Fermi level is assumed to be equal to the work function of the (metal)

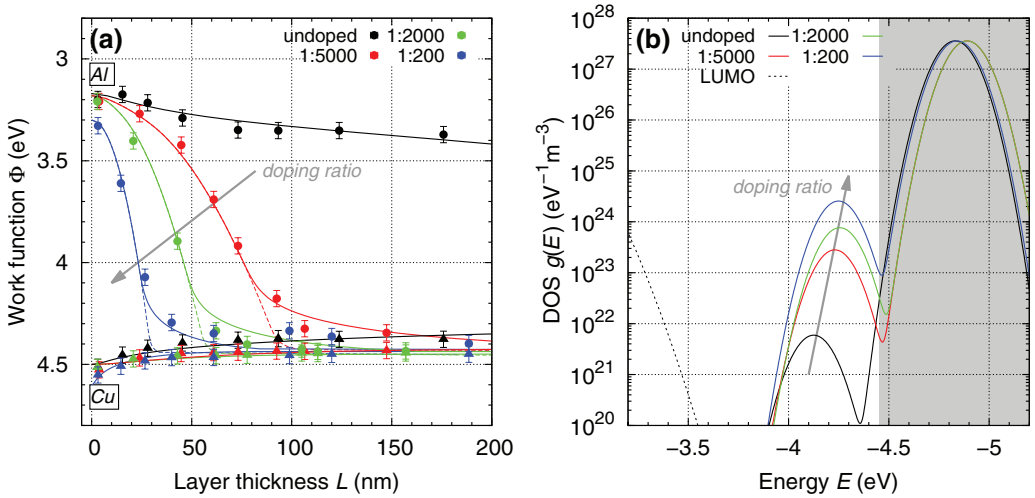

FIG. 5. (Color online) (a) Experimental data (symbols) and numerical calculated work functions (lines) of undoped and F_4TCNQ-doped P3HT layers on aluminum and copper. Numerical calculations assume Arkhipov's DOS distribution including doping-induced tail states (solid lines) or a single-Gaussian DOS shape (dashed lines). (b) Corresponding HOMO DOS distributions based on Arkhipov's model. The unshaded energy range is probed in the Kelvin probe experiment. A minor contribution of LUMO levels (dotted line) is inferred from the work-function curve of undoped P3HT on aluminum.

substrate ($\Phi_{\text{Sub}} = -E_F$). The work function at the organic semiconductor surface can be calculated by

$$\Phi_{\text{OSC}}(L) = \Phi_{\text{Sub}} - \phi(L). \tag{4}$$

Unfortunately, a direct extraction of the DOS distributions from work-function data is not possible and therefore an *a priori* assumption about its functional form is indispensable. At first, we attempt to reconstruct the work-function curves by assuming a single Gaussian-shaped $g_{\text{HOMO}}(E)$. Close reproduction the work-function data of undoped P3HT on copper, and our previous analysis of the hole mobilities in F_4TCNQ-doped P3HT layers[15] suggest to set the total density of states N to 7×10^{26} m^{-3} and the width parameter σ to 78 meV. In the work-function calculations of the doped and undoped samples, the center of the HOMO DOS distribution E_{HOMO} varies from −4.75 to −4.83 eV. For a proper description of the undoped-P3HT work-function data, a minor injection from aluminum into the tail of the P3HT LUMO distribution has been taken into account in these calculations and in the following [see Fig. 5(b)].

While the calculated work functions for layers with different thicknesses on copper (not shown) are in satisfactory agreement with the experimental data, there are distinct discrepancies for the doped P3HT layers on aluminum (dashed lines in Fig. 5). Most strikingly, the assumption of a simple Gaussian DOS shape is not in line with the long tail of the work-function curves towards saturation, which indicates that a proper description must account for doping-induced states at the low-energy tail of the DOS distribution.

The broadening of the DOS distribution due to ionized dopants has been repeatedly suggested.[23,24,45–48] Arkhipov *et al.* discussed a model that accounts for the Coulomb interaction of the doping-induced charge carriers with the left-behind ionized dopants.[23,24] In this model, the superposition of the original DOS distribution and the Coulomb wells of the ionized dopants is simplified by considering the site nearest to a dopant ion as a trap. The resulting HOMO DOS reads

$$g_{\text{HOMO}}(E) = \frac{N - N_d}{N} g_i(E) + \frac{N_d}{N} g_i\left[E - \frac{e^2}{4\pi\epsilon_0\epsilon_r a} - U_m(N_d)\right], \tag{5}$$

where N is the total site density in an undoped sample, N_d is the density of left-behind ionized (acceptor) dopants (assumed to be equal to the mobile-hole density), and $g_i(E)$ is a Gaussian-shaped DOS distribution centered at E_{HOMO} with a width of σ. The density of ionized dopants causes a reduction of the intrinsic (undoped) DOS (first term) and a subsequent formation of an equal amount of trap states shifted by the energy of the Coulomb interaction (second term). Since the DOS distribution of the undoped material is Gaussian, the distribution of the trap states is chosen to be Gaussian accordingly. Thereby, a represents the typical distance between a dopant ion and the trapped charge carrier. Physically, a should correspond to the distance between the dopant ion and an adjacent site of the semiconductor. The interaction energy is corrected for the overlap of the Coulomb potentials of neighboring dopant ions at high doping ratios by the nontrivial value of $U_m(N_d)$. For simplicity, the width parameter σ is assumed to be equal for both overlapping Gauss functions g_i. Within our previous numerical computation of hopping mobilities, Eq. (5) proved to be eligible to reproduce the doping ratio dependence of the hole mobility in F_4TCNQ-doped P3HT layers.[15] In addition, note that a Gaussian-shaped distribution of subband gap states was reported for F_4TCNQ-doped *N*,*N*'-diphenyl-*N*,*N*'-bis(1-naphthyl)-1,10-biphenyl-4,4"-diamine (α-NPD) as inferred from Kelvin probe force measurements on organic field-effect transistors.[48]

Using the DOS function from Eq. (5) and the parameters in Table III, a good agreement between the calculated and the experimental work functions is reached [see solid lines in Fig. 5(a)]. The according DOS distributions are plotted in Fig. 5(b). Most remarkably, the calculated curves feature the

TABLE III. Parameters of the DOS distributions according to Arkhipov's model, which have been used for the calculation of surface potentials in Fig. 5.[a]

Doping ratio	N_d[b] (m^{-3})	E_{HOMO}[c] (eV)
Undoped	1.16×10^{21}	−4.83
1:5000	5.5×10^{22}	−4.89
1:2000	1.5×10^{23}	−4.89
1:200	5×10^{23}	−4.94

[a]Total site density $N = 7 \times 10^{26}$ m^3, DOS width parameter $\sigma_{HOMO} =$ 78 meV, anion-trapped hole pair distance $a = 0.57$ nm.
[b]Ionized dopant density (equal to the free-hole density).
[c]Center of the bulk Gaussian distribution.

characteristic long tails before the work function saturates. Note that, for simplicity, we have fixed the values of a and σ to 0.57 nm and 78 meV, respectively, assuming that the morphology of the P3HT layer remains unchanged up to a doping ratio of 1:200, which is in line with the observations of Duong *et al.*.[49] A further improved agreement between experimental and calculated data might be achieved by relaxing these constraints or, in particular, by choosing a broader shape for the trap state distribution, being closer to the exponential-like line shape commonly observed in undoped small-molecule organic semiconductor films.[50–52] Above all, our calculations substantiate that a proper description of the gradual approach of the work function towards the bulk limit of F_4TCNQ-doped P3HT on aluminum must generally take into account that additional sites in the polymer HOMO are created via the introduction of ionized acceptor molecules. The accuracy of this approach is supported by the good agreement between the density of these sites determined from the fits at larger thicknesses and the value for the ionized acceptor concentration extracted from the initial parabolic shape at smaller film thickness. In conformity with the interpretation of the absorption data, we do not see a significant amount of LUMO states that could stem from the formation of hybrid charge transfer complexes. If such species were formed between F_4TCNQ and P3HT in the vicinity of the aluminum bottom electrode, we should observe a rather sudden increase of the work function from Φ_{Al} to the level of those LUMO states according to the density of applied F_4TCNQ acceptor molecules.

Free-hole densities (equivalent to the densities of ionized F_4TCNQ molecules that yield mobile holes) derived from the simulations are given in Table III and plotted as a function of the doping ratio in Fig. 6. We observe that the charge density in the depletion zone is only approximately 5% of the present F_4TCNQ molecules. These values complement well the free-hole densities which we have independently determined from our previous capacitance-voltage (C-V) measurements on layers in a metal-insulator-semiconductor (MIS) geometry (see Fig. 6).[15] Note that the coincidence of the free-hole densities from Kelvin probe and C-V measurements on different sample geometries including various metal electrodes substantiates that these densities are characteristic for the bulk of the doped layers. Since we have shown above that almost every F_4TCNQ is ionized, this implies that only every twentieth ionization event creates a mobile hole that can diffuse to the polymer/Al interface, and that can thus contribute to the Fermi level alignment in the samples on aluminum.

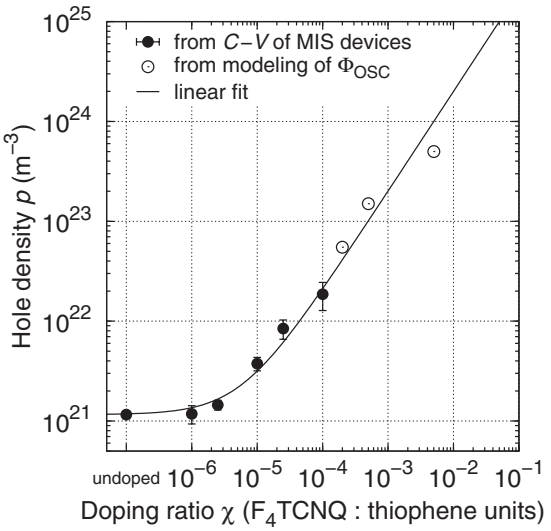

FIG. 6. Free-hole densities as determined by C-V measurements of layers in MIS geometry (see our previous work, Ref. 15) and by numerical modeling of the thickness dependence of the work function of F_4TCNQ-doped P3HT layers on metal substrates. The line corresponds to the linear function $p = 2.0 \times 10^{26}$ $m^{-3}\chi + 1.2 \times 10^{21}$ m^{-3}.

The observation that approximately 95% of the hole-F_4TCNQ anion pairs are bound may be explained by the low permittivity of hydrocarbon-based semiconductors. Assuming that a purely thermal activation process causes free charge carrier formation via charge-pair dissociation requires an activation energy of 77 meV at a temperature of 300 K, which is much lower than the typical exciton binding energy of 0.2–0.5 eV in organic semiconductors.[1] A recent simulation of Mityashin *et al.* indicates that the splitting of these charge pairs is favored by dissociation pathways within the energetic landscape of transport sites which might resolve this discrepancy.[53] According to Mityashin and co-workers, however, these pathways are due to the electrostatic interaction of neighboring charge pairs, which implies a doping ratio dependent dissociation efficiency and, in particular, that almost no dissociation occurs at low doping ratios. This is in clear contrast to our observation that the dissociation efficiency is constantly 5% in a broad range of doping concentrations, including very low doping ratios.

C. Electrical conductivity and free-hole mobility

The electrical conductivities of undoped and F_4TCNQ-doped P3HT layers are shown in Fig. 7. Part of the data stem from our previous analysis of the admittance spectra of MIS devices.[15] We consolidate this data with current-voltage (I-V) measurements of hole-only devices. The respective I-V characteristics show a symmetric and linear behavior around 0 V and up to $|V| \approx 1$ V. At high doping ratios, the hole-only conductivities connect well to the previous data. The undoped and weakly doped samples suffer from an increased conductivity, which is probably due to the degradation of the polymer sample during the more-than-one-year delay between the I-V and the previous admittance measurements. To support this interpretation, we repeated the admittance measurement of a freshly prepared undoped P3HT layer in the

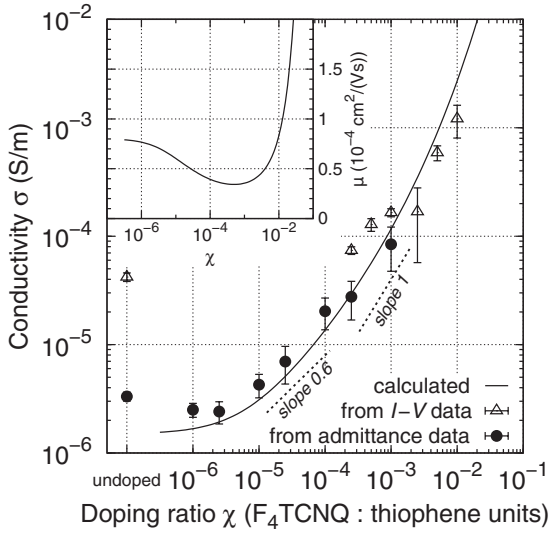

FIG. 7. Conductivities as determined by admittance measurements of layers in MIS geometry (solid symbols)[15] and *I-V* measurements of hole-only devices (open symbols). The line is the predicted conductivity based on the mobility model by Arkhipov *et al.*[23,54] and the hole densities from Fig. 6. The inset shows the calculated mobility values.

MIS geometry, and this experiment yielded increased values of the free-hole density and bulk conductivity as compared to the data published previously.

The measured conductivities increase monotoneously and nonlinearly with increasing doping ratio. This implies, in conjunction with a strictly linear increase of the free-hole density upon doping, a rather complicated relationship between the doping ratio and the hole mobility. In particular, we find a sublinear increase of the conductivity at low to moderate doping ratios ($\chi < 10^{-4}$), which means that the mobility decreases in this regime. At higher doping ratios, the conductivity increase is superlinear and, thus, linked with an increase of the free-hole mobility.

Our updated calculations of mobility and conductivity using the mobility model for doped organic semiconductors of Arkhipov *et al.*[23,54] agree excellently with the extended experimental data in the full range of doping ratios (see Fig. 7). Note that we have used similar parameters as in our previous work (see Table IV) and the same DOS distributions as in the above simulation of the work function curves (i.e., the same values for N, σ, and a).

Following the model of Arkhipov and co-workers, we explain the mobility decrease at low to moderate doping ratios with the broadening of the DOS distribution by the attracting Coulomb potentials of the ionized F_4TCNQ molecules [see Fig. 5(b)]. The occurrence of these Coulombic traps counteracts the fill-up of the low-mobility tail of the DOS distribution upon doping. At the low-to-moderate doping regime, this can lead to a reduction of the mobility as seen here. At higher doping ratios, the Coulomb potentials of individual ionized F_4TCNQ dopants overlap such that the effective barrier for the release of trapped holes is lowered. This is accounted for by the term $U_m(N_d)$ in Eq. (5). As a consequence, the mobility becomes increasingly controlled by the fill-up of the DOS distribution in the strong doping regime and, hence, increases.

TABLE IV. Parameters used in the calculations of the free-hole mobility and conductivity in Fig. 7.

Total density of states N	7×10^{26} m^{-3}
DOS width parameter σ	78 meV
Anion-trapped hole pair distance a	0.57 nm
Inverse hole localization radius γ	2.9 nm^{-1}
Attempt-to-hop frequency ν_0	3×10^{12} s^{-1}
Electric field F	2×10^4 V m^{-1}
Temperature T	300 K

IV. SUMMARY

In summary, we derived a conclusive picture of the ionized-dopant and free-charge carrier formation in P3HT doped with F_4TCNQ. In this system, charge transfer is very efficient and leads to a full onefold ionization of both the donor and acceptor moieties. Thereby the majority of the F_4TCNQ dopants undergoes charge transfer, ruling out significant formation of isolated domains of neutral F_4TCNQ. However, most of the charge carrier pairs remain strongly bound and are not available for electrical conduction. Dissociation, which occurs for only 5% of these pairs, might be favored by dissociation pathways through the energetic distribution of transport sites.

As a consequence of charge carrier pair dissociation, doped layers exhibit an increased density of mobile holes. The corresponding electrons remain localized at the F_4TCNQ dopants, which are dispersed in the P3HT matrix. Due to the low permittivity, the Coloumb potentials of the ionized F_4TCNQ molecules have a rather long range and therefore affect the energetic and charge transport properties of the layer. We have shown that the HOMO-derived density-of-states distribution of P3HT is broadened upon doping with F_4TCNQ and that this broadening serves to explain the complex conductivity-doping ratio relationship. In particular, the presence of F_4TCNQ anions leads to a decrease of the hole mobility at low to moderate doping ratios.

Finally, we would like to point out that the integer charge transfer mechanism of P3HT and F_4TCNQ may not be anticipated for conjugated organic donors and acceptors in general. Intermolecular electronic interactions depend critically on the overlap of the relevant wave functions and are governed by the minimization of energy. Therefore partial charge transfer, i.e., the formation of hybrid charge transfer complexes, may occur for other donor-acceptor pairs as suggested in literature. The possible variety of doping mechanisms has to be considered when investigating organic semiconductor doping-related phenomena.

ACKNOWLEDGMENTS

Thanks are due to Peter Brückner for the surface potential measurements, Dr. Jan Behrends (Freie Universität Berlin) and Prof. Alberto Salleo (Stanford University) for stimulating discussions, and Prof. Ullrich Scherf (Universität Wuppertal) for providing the P3HT sample. This work has been financially supported by the German Ministry of Education and Research (NeMO FKZ 13N10622, PVcomB FKZ 03IS2151D).

*neher@uni-potsdam.de

[1] K. Walzer, B. Maennig, M. Pfeiffer, and K. Leo, Chem. Rev. **107**, 1233 (2007).

[2] W. Y. Gao and A. Kahn, Appl. Phys. Lett. **79**, 4040 (2001).

[3] M. Pfeiffer, A. Beyer, T. Fritz, and K. Leo, Appl. Phys. Lett. **73**, 3202 (1998).

[4] W. Y. Gao and A. Kahn, J. Appl. Phys. **94**, 359 (2003).

[5] B. Maennig, M. Pfeiffer, A. Nollau, X. Zhou, K. Leo, and P. Simon, Phys. Rev. B **64**, 195208 (2001).

[6] H. Kleemann, B. Lussem, and K. Leo, J. Appl. Phys. **111**, 123722 (2012).

[7] E. F. Aziz, A. Vollmer, S. Eisebitt, W. Eberhardt, P. Pingel, D. Neher, and N. Koch, Adv. Mater. **19**, 3257 (2007).

[8] J. Hwang and A. Kahn, J. Appl. Phys. **97**, 103705 (2005).

[9] E. Lim, B. J. Jung, M. Chikamatsu, R. Azumi, Y. Yoshida, K. Yase, L. M. Do, and H. K. Shim, J. Mater. Chem. **17**, 1416 (2007).

[10] L. Ma, W. H. Lee, Y. D. Park, J. S. Kim, H. S. Lee, and K. Choa, Appl. Phys. Lett. **92**, 063310 (2008).

[11] J. Sun, B. J. Jung, T. Lee, L. Berger, J. Huang, Y. Liu, D. H. Reich, and H. E. Katz, ACS Appl. Mater. Interfaces **1**, 412 (2009).

[12] K. H. Yim, G. L. Whiting, C. E. Murphy, J. J. M. Halls, J. H. Burroughes, R. H. Friend, and J. S. Kim, Adv. Mater. **20**, 3319 (2008).

[13] Y. Zhang, B. de Boer, and P. W. M. Blom, Adv. Funct. Mater. **19**, 1901 (2009).

[14] Y. Zhang and P. W. M. Blom, Appl. Phys. Lett. **97**, 083303 (2010).

[15] P. Pingel, R. Schwarzl, and D. Neher, Appl. Phys. Lett. **100**, 143303 (2012).

[16] P. Pingel, L. Y. Zhu, K. S. Park, J. O. Vogel, S. Janietz, E. G. Kim, J. P. Rabe, J. L. Brédas, and N. Koch, J. Phys. Chem. Lett. **1**, 2037 (2010).

[17] S. G. Chen, P. Stradins, and B. A. Gregg, J. Phys. Chem. B **109**, 13451 (2005).

[18] J.-H. Lee, H.-M. Kim, K.-B. Kim, R. Kabe, P. Anzenbacher, Jr., and J.-J. Kim, Appl. Phys. Lett. **98**, 173303 (2011).

[19] M. L. Tietze, L. Burtone, M. Riede, B. Lussem, and K. Leo, Phys. Rev. B **86**, 035320 (2012).

[20] B. A. Gregg, S. G. Chen, and R. A. Cormier, Chem. Mater. **16**, 4586 (2004).

[21] I. Salzmann, G. Heimel, S. Duhm, M. Oehzelt, P. Pingel, B. M. George, A. Schnegg, K. Lips, R.-P. Blum, A. Vollmer, and N. Koch, Phys. Rev. Lett. **108**, 035502 (2012).

[22] L. Zhu, E.-G. Kim, Y. P. Yi, and J. L. Brédas, Chem. Mater. **23**, 5149 (2011).

[23] V. I. Arkhipov, E. V. Emelianova, P. Heremans, and H. Bässler, Phys. Rev. B **72**, 235202 (2005).

[24] V. I. Arkhipov, P. Heremans, E. V. Emelianova, and H. Bässler, Phys. Rev. B **71**, 045214 (2005).

[25] A. Zen, M. Saphiannikova, D. Neher, J. Grenzer, S. Grigorian, U. Pietsch, U. Asawapirom, S. Janietz, U. Scherf, I. Lieberwirth, and G. Wegner, Macromolecules **39**, 2162 (2006).

[26] P. Pingel, A. Zen, R. D. Abellon, F. C. Grozema, L. D. A. Siebbeles, and D. Neher, Adv. Funct. Mater. **20**, 2286 (2010).

[27] A. Zen, J. Pflaum, S. Hirschmann, W. Zhuang, F. Jaiser, U. Asawapirom, J. P. Rabe, U. Scherf, and D. Neher, Adv. Funct. Mater. **14**, 757 (2004).

[28] M. M. Beerbom, B. Lagel, A. J. Cascio, B. V. Doran, and R. Schlaf, J. Electron Spectrosc. Relat. Phenom. **152**, 12 (2006).

[29] P. J. Brown, H. Sirringhaus, M. Harrison, M. Shkunov, and R. H. Friend, Phys. Rev. B **63**, 125204 (2001).

[30] R. Österbacka, C. P. An, X. M. Jiang, and Z. V. Vardeny, Science **287**, 839 (2000).

[31] J. B. Torrance, J. J. Mayerle, K. Bechgaard, B. D. Silverman, and Y. Tomkiewicz, Phys. Rev. B **22**, 4960 (1980).

[32] D. A. Dixon, J. C. Calabrese, and J. S. Miller, J. Phys. Chem. **93**, 2284 (1989).

[33] C. G. Shuttle, B. O'Regan, A. M. Ballantyne, J. Nelson, D. D. C. Bradley, and J. R. Durrant, Phys. Rev. B **78**, 113201 (2008).

[34] J. M. Guo, H. Ohkita, H. Benten, and S. Ito, J. Am. Chem. Soc. **132**, 6154 (2010).

[35] I. A. Howard, R. Mauer, M. Meister, and F. Laquai, J. Am. Chem. Soc. **132**, 14866 (2010).

[36] D. Herrmann, S. Niesar, C. Scharsich, A. Köhler, M. Stutzmann, and E. Riedle, J. Am. Chem. Soc. **133**, 18220 (2011).

[37] See Supplemental Material at http://link.aps.org/supplemental/10.1103/PhysRevB.87.115209 for a discussion of the P3HT polaron and F_4TCNQ anion reference spectra, example reconstructions of the NIR absorption spectra of F_4TCNQ-doped P3HT in chloroform at various solution concentrations, and I-V characteristics of F_4TCNQ-doped P3HT hole-only devices.

[38] O. D. Parashchuk, A. Y. Sosorev, V. V. Bruevich, and D. Y. Paraschuk, JETP Lett. **91**, 351 (2010).

[39] T. J. Prosa, M. J. Winokur, J. Moulton, P. Smith, and A. J. Heeger, Macromolecules **25**, 4364 (1992).

[40] Y. A. Zhang and P. W. M. Blom, Org. Electron. **11**, 1261 (2010).

[41] C. B. Duke, W. R. Salaneck, T. J. Fabish, J. J. Ritsko, H. R. Thomas, and A. Paton, Phys. Rev. B **18**, 5717 (1978).

[42] C. B. Duke and T. J. Fabish, Phys. Rev. Lett. **37**, 1075 (1976).

[43] I. Lange, J. C. Blakesley, J. Frisch, A. Vollmer, N. Koch, and D. Neher, Phys. Rev. Lett. **106**, 216402 (2011).

[44] H. Ishii, N. Hayashi, E. Ito, Y. Washizu, K. Sugi, Y. Kimura, M. Niwano, Y. Ouchi, and K. Seki, Phys. Status Solidi A **201**, 1075 (2004).

[45] Y. L. Shen, K. Diest, M. H. Wong, B. R. Hsieh, D. H. Dunlap, and G. G. Malliaras, Phys. Rev. B **68**, 081204 (2003).

[46] A. Dieckmann, H. Bässler, and P. M. Borsenberger, J. Chem. Phys. **99**, 8136 (1993).

[47] G. Garcia-Belmonte, E. V. Vakarin, J. Bisquert, and J. P. Badiali, Electrochim. Acta **55**, 6123 (2010).

[48] O. Tal, Y. Rosenwaks, Y. Preezant, N. Tessler, C. K. Chan, and A. Kahn, Phys. Rev. Lett. **95**, 256405 (2005).

[49] D. T. Duong, C. C. Wang, E. Antono, M. F. Toney, and A. Salleo, Org. Electron. (2013), doi:10.1016/j.orgel.2013.02.028.

[50] T. Sueyoshi, H. Fukagawa, M. Ono, S. Kera, and N. Ueno, Appl. Phys. Lett. **95**, 183303 (2009).

[51] W. L. Kalb, S. Haas, C. Krellner, T. Mathis, and B. Batlogg, Phys. Rev. B **81**, 155315 (2010).

[52] S. Olthof, S. Mehraeen, S. K. Mohapatra, S. Barlow, V. Coropceanu, J.-L. Brédas, S. R. Marder, and A. Kahn, Phys. Rev. Lett. **109**, 176601 (2012).

[53] A. Mityashin, Y. Olivier, T. Van Regemorter, C. Rolin, S. Verlaak, N. G. Martinelli, D. Beljonne, J. Cornil, J. Genoe, and P. Heremans, Adv. Mater. **24**, 1535 (2012).

[54] V. I. Arkhipov, P. Heremans, E. V. Emelianova, G. J. Adriaenssens, and H. Bässler, Appl. Phys. Lett. **82**, 3245 (2003).